Multibody Syst Dyn (2009) 21: 325–345
DOI 10.1007/s11044-008-9141-3

An improved dynamic modeling of a multibody system with spherical joints

Ali Rahmani Hanzaki · Subir Kumar Saha · P.V.M. Rao

Received: 5 December 2007 / Accepted: 13 November 2008 / Published online: 8 January 2009

Abstract A dynamic modeling of multibody systems having spherical joints is reported in this work. In general, three intersecting orthogonal revolute joints are substituted for a spherical joint with vanishing lengths of intermediate links between the revolute joints. This procedure increases sizes of associated matrices in the equations of motion, thus increasing computational burden of an algorithm used for dynamic simulation and control. In the proposed methodology, Euler parameters, which are typically used for representation of a rigid-body orientation in three-dimensional Cartesian space, are employed to represent the orientation of a spherical joint that connects a link to its previous one providing three-degree-of-freedom motion capability. For the dynamic modeling, the concept of the Decoupled Natural Orthogonal Complement (DeNOC) matrices is utilized. It is shown in this work that the representation of spherical joints motion using Euler parameters avoids the unnecessary introduction of the intermediate links, thereby no increase in the sizes of the associated matrices with the dynamic equations of motion. To confirm the efficiency of the proposed representation, it is illustrated with the dynamic modeling of a spatial four-bar Revolute-Spherical–Spherical-Revolute (RSSR) mechanism, where the CPU time of the dynamic modeling based on proposed methodology is compared with that based on the revolute joints substitution. Finally, it is explained how a complex suspension and steering linkage can be modeled using the proposed concept of Euler parameters to represent a spherical joint.

A. Rahmani Hanzaki (✉)
Mechanical Engineering Dept., Shahid Rajaee University, Lavizan, Tehran, Iran
e-mail: rahmaniali47@yahoo.com

A. Rahmani Hanzaki
e-mail: a.rahmani@srttu.edu

S.K. Saha · P.V.M. Rao
Mechanical Engineering Dept., IIT Delhi, Hauz Khas, New Delhi, 110016, Delhi, India

S.K. Saha
e-mail: saha@mech.iitd.ac.in

P.V.M. Rao
e-mail: pvmrao@mech.iitd.ac.in

Keywords Spherical joint · Dynamic modeling · Euler parameters · Closed loop

1 Introduction

Dynamic analysis of multibody systems, e.g., robot manipulators and mechanisms, plays an important role in investigation of their performances. The analysis consists of two branches, which are: (i) Forward dynamics, where the forces acting on a mechanical system are known and the equations of motion of the system are solved to obtain the motion of the system in terms of linear and angular positions, velocities, and accelerations; (ii) Inverse dynamics, in which the motion of each link is known and the aim is to find the forces required at the joints to achieve the desired motion [1]. To perform the dynamics study, one requires kinematic analysis, where an appropriate choice of the rotation representation of a rigid link is important, particularly, for three-degree-of-freedom (DOF) motion of a rigid-body. Three common rotational coordinates are: Euler angles, Euler parameters, and direction cosines. Amongst all three, the Euler parameters have many advantages over both the Euler angles and the direction cosines representations. Some of the advantages are that there is no inherent geometrical singularity, and there is no orientation of a body for which the Euler parameters cannot be defined. In addition, the rotation matrix using Euler parameters is free of trigonometric functions in opposed of that using Euler angles. However, they are dependent, as four variables are required to define any 3-DOF spatial rotation [1, 2].

Euler parameters are defined based on the Euler theorem [1], which states that the orientation of a body with one point fixed can be defined by its rotation about an imaginary axis by an angle β at any instant of time t. Accordingly, the Euler parameters are established as

$$e_0 = \cos(\beta/2); \qquad \mathbf{e} = \mathbf{u}\sin(\beta/2); \qquad \mathbf{p_e} \equiv \begin{bmatrix} e_0 & \mathbf{e}^{\mathrm{T}} \end{bmatrix}^{\mathrm{T}} \tag{1}$$

where $\mathbf{u}$ is the imaginary axis about which the rotation of the body or a frame attached to it happens. From (1), it is obvious that sum of the square of Euler parameters is equal to one. In other words,

$$\mathbf{p}_\mathbf{e}^{\mathrm{T}}\mathbf{p_e} = 1 \tag{2}$$

The rotation matrix, $\mathbf{B}$, based on the Euler parameters, is thus obtained as [1]

$$\mathbf{B} = \left(2e_0^2 - 1\right)\mathbf{1} + 2\left(\mathbf{e}\mathbf{e}^{\mathrm{T}} + e_0\tilde{\mathbf{e}}\right) \tag{3}$$

in which, $\mathbf{1}$ is the 3×3 identity matrix and $\tilde{\mathbf{e}}$ is a skew-symmetric matrix associated with vector $\mathbf{e}$ such that $\tilde{\mathbf{e}}\mathbf{x} = \mathbf{e} \times \mathbf{x}$, for any 3-dimensional Cartesian vector, $\mathbf{x}$. This is called cross-product matrix in the paper to follow some literature like [3, 4]; however, that is identified spin-tensor in some other literature. Hence, matrix $\tilde{\mathbf{e}}$ is represented as

$$\tilde{\mathbf{e}} = \begin{bmatrix} 0 & -e_3 & e_2 \\ e_3 & 0 & -e_1 \\ -e_2 & e_1 & 0 \end{bmatrix} \tag{4}$$

Angular velocity of the body is then derived using the derivatives of the above Euler parameters as [1]

$$\boldsymbol{\omega} = 2\mathbf{G}\dot{\mathbf{p}}_\mathbf{e} \tag{5}$$

where $\boldsymbol{\omega}$ is the angular velocity of the body, whereas $\dot{\mathbf{p}}_\mathbf{e} \equiv [\dot{e}_0, \dot{\mathbf{e}}^\mathrm{T}]^\mathrm{T}$ is the first derivatives of the Euler parameters and $\mathbf{G} \equiv [-\mathbf{e}, \tilde{\mathbf{e}} + e_0\mathbf{1}]$.

For dynamic modeling, two popular approaches used are (i) Newton–Euler (NE), and (ii) the Euler–Lagrange (EL) formulations [2]. The NE formulation in its original form is straightforward and is able to find all of the forces including the reactions that are not essential for simulation, i.e., the study of motions. Hence, this approach is not preferred for the simulation of large systems. Alternatively, EL approach provides equations of motion without the reaction forces. Hence, it is a simplified approach for simulation, but requires complex partial derivatives. As a bridge between the above two formulations, i.e., one starts with NE formulation and ends up with EL equations, several methods based on the orthogonal complements to the velocity constraint matrix have been proposed [5, 6]. One such methodology uses the Decoupled Natural Orthogonal Complement (DeNOC) matrices [3] that was originally proposed for serial rigid manipulator, but was later extended to parallel [4] and general closed-loop systems [7] as well. One of the major advantages of using the DeNOC matrices is the availability of recursive dynamics even for general closed-loop systems. In the past, the use of the DeNOC matrices was presented for a mechanical system, open or closed, with one-DOF revolute or prismatic joints only. In the presence of higher DOF joints, namely cylindrical or spherical, they were treated as a combination of revolute-prismatic or three intersecting revolute joints, respectively. For example, in [8], the twist of a link connected to its previous one is given using three intersecting revolute joints. Moreover, the kinematics of spatial revolute-spherical–spherical-revolute (RSSR) linkage was analyzed in [9] by treating the spherical joints as three orthogonally intersecting revolute joints. The dynamics of the same linkage was modeled in [7] using the kinematics results of [9] and the DeNOC matrices. Such considerations cause an increase in the sizes of associated matrices arising out of kinematics and dynamics modeling, thereby causing inefficiencies in the resulting algorithms. Hence, the use of Euler parameters to represent the motion of a spherical joint is proposed in [10]. Since spherical joint has many usages in mechanisms, it has been studied in many articles. Robertson and Slocum developed a high stiffness spherical joint capable of a large, singular free workspace [11]. The utilized three frames to represent the relative location of the roll, pitch, and yaw axes of the spherical joint. Attia studied a car suspension system [12] and a general serial chain [13], which have several spherical joints.

In this paper, a spherical joint allowing three-DOF rotation is studied using Euler parameters. The resultant algorithm has reduced matrix sizes, which increases the efficiency of the algorithm. To demonstrate this, the RSSR linkage studied in [7, 9] is analyzed, and the CPU time for the inverse dynamics of the RSSR linkage is compared with those based on the algorithm presented in [7]. The comparison proves the improved efficiency of the proposed methodology. Finally, dynamic modeling of a suspension and steering linkage, as a multiloop mechanism consists of several spherical joints, is described briefly.

This paper is organized as follows. Section 2 shows the kinematic analysis of a general closed chain in detail considering the necessities of its dynamic modeling. In Sect. 3, the DeNOC matrices, which were derived elsewhere for systems with only one-DOF revolute/prismatic joints and explained in the Appendix, are improved for a body connected to its previous one with a spherical joint and then the structure of the matrices for a multiloop chain is presented. The proposed methodology in Sects. 2 and 3 is employed in Sect. 4 to analyze an RSSR (Revolute-Spherical–Spherical-Revolute) linkage, as an example, and the CPU time of this analysis is compared with same problem solved using revolute joints substitution. The complex linkage of suspension and steering system is also discussed in order to demonstrate its modeling by use of the proposed concept of Euler parameters to represent a spherical joint motion, followed by the conclusions in Sect. 5.

The main contribution of this paper is to derive the DeNOC matrices for a multibody system with one or some spherical joints by the use of Euler parameters.

2 Kinematic modeling

To illustrate the use of the Euler parameters to represent the spherical joint motion, a generalized closed-loop chain shown in Fig. 1(a) is considered whose links are numbered as #1, . . . , #h. The method of numbering will be discussed later. Using the Kutzbach criterion [14], the degree of freedom (DOF) of the linkage can be found. Note that the existence of a link connected to neighboring links with just two spherical joints causes a redundant-DOF, which is the rotation of the link about its axis joining the centers of the spherical joints and must be considered when the constraint equations are formulated. To find the number of independent loops, the following simple expression can be used:

$$\text{number of loops} = \text{number of joints} - \text{number of bodies} \tag{6}$$

On the other hand, one needs the topology of the linkage obtained from graph theory [15–19] to find the best joints to be cut. Figure 1(b) shows a typical topology for the system shown in Fig. 1(a). In this figure, the circles show the links, where the lines connecting the circles are the indicators of the joints. Furthermore, a Cartesian coordinate is attached to every link at its joint to describe the motion of the next consecutive link. The x-axis of this coordinate is always taken along the link axis, while its z-axis is along the joint axis for one-DOF revolute or prismatic joint. For the spherical joints, the direction of z-axis will be discussed subsequently.

2.1 Kinematic constraints for a closed-loop system

Now, the constraint equations are formulated as follows:

- Three scalar equations for every loop-closure equation. As it is shown in Fig. 1(a), two proper joints, e.g., 1 and $h+1$ of Fig. 1(a), are connected by a vector virtually. The vector is calculated from two different paths like 1–2–3–. . .–$(h+1)$ and f–$(f+1)$–$(f+2)$–. . .–$(h+1)$ of the closed loop. Equating the two, gives a vectorial loop closure equation, whose three components are used here as three constraint equations;
- The dependency equations of the Euler parameters, i.e., (2);

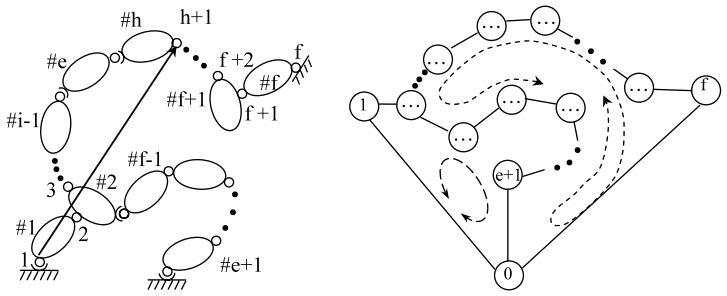

(a) Closed-loop system (b) Topology of the system

Fig. 1 A general closed-loop system

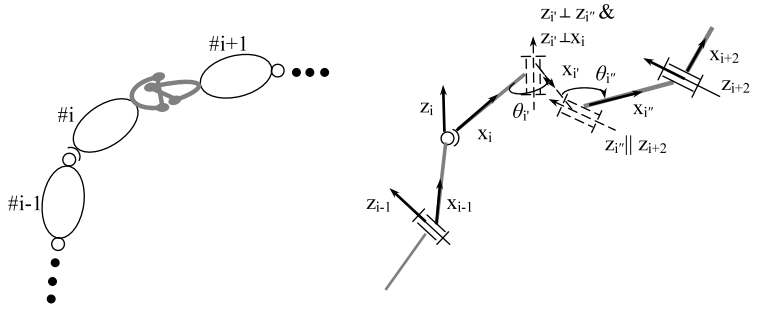

(a) A part of linkage with substituted joint

(b) A pair of two orthogonal revolute joints instead of a Hooke joint

Fig. 2 Substitution of a spherical joint with a Hooke joint

- Constraint equations to eliminate the redundant DOFs between every two spherical joints connected by a link. In such situation, two orthogonal intersecting revolute joints, representing a Hooke joint are considered to replace the spherical joint, as indicated in Fig. 2. The length of the imaginary link, i.e., #*i*', is taken as zero. To write the mathematical expression of this constraint, the rotation of the *i*th frame in fixed frame is constant from right side or from left side of the chain. This constraint is explained in detail for an RSSR linkage in Sect. 4.

Now, these constraint equations are expressed in vector form as

$$\boldsymbol{\varphi}(\mathbf{q}) = \mathbf{0} \tag{7}$$

where $\mathbf{q} \equiv [\mathbf{o}^{\mathrm{T}}\ \mathbf{r}^{\mathrm{T}}]^{\mathrm{T}}$ is the vector of generalized coordinates of $\mathbf{o}$ and $\mathbf{r}$ representing the vectors of unknown and known variables, respectively. This partitioning helps one to solve (8) for the generalized speeds presenting the time derivatives of generalized coordinates easily. To derive the angular velocities, the constraint equations, namely (7) is differentiated with respect to time, i.e.,

$$\boldsymbol{\Phi}_{\mathbf{o}}\dot{\mathbf{o}} + \boldsymbol{\Phi}_{\mathbf{r}}\dot{\mathbf{r}} = \mathbf{0} \tag{8}$$

in which, $\boldsymbol{\Phi}_{\mathbf{o}} \equiv [\partial\boldsymbol{\varphi}/\partial\mathbf{o}]$; $\boldsymbol{\Phi}_{\mathbf{r}} \equiv [\partial\boldsymbol{\varphi}/\partial\mathbf{r}]$; and $\dot{\mathbf{o}}$ and $\dot{\mathbf{r}}$ are the time derivatives of $\mathbf{o}$ and $\mathbf{r}$, respectively [1]. The acceleration expressions are similarly obtained by differentiating the velocity expressions, namely (8), which is written in a compact form as

$$\boldsymbol{\Phi}_{\mathbf{o}}\ddot{\mathbf{o}} + \boldsymbol{\Phi}_{\mathbf{r}}\ddot{\mathbf{r}} + (\boldsymbol{\Phi}_{\mathbf{q}}\dot{\mathbf{q}})_{\mathbf{q}}\dot{\mathbf{q}} = \mathbf{0} \tag{9}$$

where $(\boldsymbol{\Phi}_{\mathbf{q}}\dot{\mathbf{q}})_{\mathbf{q}} \equiv \partial(\boldsymbol{\Phi}_{\mathbf{q}}\dot{\mathbf{q}})/\partial\mathbf{q}$, and $\boldsymbol{\Phi}_{\mathbf{q}}$ is an $m \times n$ matrix, in which m and n are the number of dependent variables, or the number of constraint equations, and the total number of variables that includes independent and dependent variables, respectively. Since $\dot{\mathbf{q}}$ is not dependent on $\mathbf{q}$ explicitly, (9) can be rewritten as

$$\boldsymbol{\Phi}_{\mathbf{o}}\ddot{\mathbf{o}} + \boldsymbol{\Phi}_{\mathbf{r}}\ddot{\mathbf{r}} + (\boldsymbol{\Phi}_{\mathbf{qq}}\dot{\mathbf{q}})\dot{\mathbf{q}} = \mathbf{0} \tag{10}$$

in which $\boldsymbol{\Phi}_{\mathbf{q}} \equiv \frac{\partial\boldsymbol{\phi}}{\partial\mathbf{q}}$ and $\boldsymbol{\Phi}_{\mathbf{qq}} \equiv \frac{\partial\boldsymbol{\Phi}_{\mathbf{q}}}{\partial\mathbf{q}}$. In view of the fact that $\boldsymbol{\Phi}_{\mathbf{q}}$ is a matrix, its each column is differentiated w.r.t. $\mathbf{q}$ and expanded in the third dimension. Therefore, $\boldsymbol{\Phi}_{\mathbf{qq}}$ is $m \times$

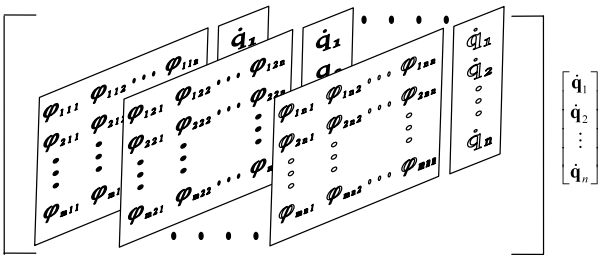

Fig. 3 Use of 3-dimensional matrix for generalized acceleration calculation

$n \times n$ matrix whose each element is $\phi_{ijk} \equiv \frac{\partial^2 \phi_i}{\partial \mathbf{q}_j \partial \mathbf{q}_k}$. Such 3-dimensional matrix can be easily handled in MATLAB software environment. The computation of $(\mathbf{\Phi_{qq}}\dot{\mathbf{q}})\dot{\mathbf{q}}$ in (10), for a system with m constraint equations and n variables [10] is shown in Fig. 3.

3 Equations of motion

The dynamics formulation of an n-link open-chain serial system with only one DOF joint (Fig. 13) using the Decoupled Natural Orthogonal Complement (DeNOC) matrices [3], which forms the basis for the modeling of the closed-loop system with h links, is outlined in the Appendix.

The twist and wrench of the ith body moving in the 3-dimensional Cartesian space are defined in the Appendix as the 6-dimensional vectors of

$$\mathbf{t}_i \equiv \begin{bmatrix} \boldsymbol{\omega}_i \\ \mathbf{v}_i \end{bmatrix} \quad \text{and} \quad \mathbf{w}_i \equiv \begin{bmatrix} \mathbf{n}_i \\ \mathbf{f}_i \end{bmatrix} \tag{11}$$

where $\boldsymbol{\omega}_i$ and $\mathbf{v}_i$ are the 3-dimensional vectors of angular velocity and linear velocity of point O_i of the ith body, respectively, whereas $\mathbf{n}_i$ and $\mathbf{f}_i$ are the 3-dimensional vectors of the resultant moment about O_i, and the resultant force at O_i, respectively.

Now in the presence of a spherical joint, where the rotation of one body w.r.t. its previous one is defined using the Euler parameters, the corresponding twist expression similar to (48) will be derived. The key point in (48) is that the joint-motion propagation matrix is associated to the number of variables signifying the degree of freedom of the joint. For the revolute and prismatic joints, $\mathbf{p}$ is a vector with size of 6×1. For the spherical joint, it should then be 6×3, as a spherical joint allows 3-DOF motion of the ith link w.r.t. its previous one. Hence, (5) cannot be used because $\dot{\mathbf{p}}_\mathbf{e}$ has four variables. An alternative representation of $\boldsymbol{\omega}$ in terms of the time rates of the 3-dimensional vector $\mathbf{e}$ as in (1) is sought. This is suitable for the derivation of dynamic equations of motion using the DeNOC matrices. For that, $\dot{\mathbf{p}}_\mathbf{e}$ of (5) is expressed first in terms of $\dot{\mathbf{e}}$ as

$$\dot{\mathbf{p}}_\mathbf{e} = \mathbf{C}\dot{\mathbf{e}} \tag{12}$$

where $\mathbf{C} \equiv [-\mathbf{e}/e_0, \mathbf{1}]^{\mathrm{T}}$. Upon substitution of (12) into (5), one obtains

$$\boldsymbol{\omega} = 2\mathbf{G}\mathbf{C}\dot{\mathbf{e}} \equiv \mathbf{G}^*\dot{\mathbf{e}} \tag{13}$$

Equation (13) is rewritten with appropriate subscripts to denote the relative angular velocity of the ith body w.r.t. the $(i-1)$st one in $(i-1)$st moving frame as

$$\boldsymbol{\omega}_{i,i-1} = \mathbf{G}_i^*\dot{\mathbf{e}}_i \tag{14}$$

in which $\mathbf{G}_i^* \equiv [\mathbf{B}_{i,i-1} + \mathbf{1}]/e_{0i}$, and e_{0i} and $\mathbf{e}_i$ are the Euler parameters representing the orientation of the ith body w.r.t. the $(i-1)$st one and $\mathbf{B}_{i,i-1}$ is the rotation matrix that transforms a vector from the frame connected to the ith body into the frame connected to the $(i-1)$st body. Equation (48) is then rewritten for the two bodies coupled by a spherical joint as

$$\mathbf{t}_i = \mathbf{A}_{i,i-1}\mathbf{t}_{i-1} + \mathbf{P}_i\dot{\mathbf{e}}_i \tag{15}$$

where the expression of the 6×6 matrix $\mathbf{A}_{i,i-1}$ is same as that in (49), whereas the 6×3 joint-motion propagation matrix is given as

$$\mathbf{P}_i \equiv \begin{bmatrix} \mathbf{G}_i^* \\ \mathbf{O} \end{bmatrix} \tag{16}$$

As pointed out in the Appendix, the generalized twist of the entire system, $\mathbf{t}$, for the n rigid bodies in the system is written in form of (50). In the presence of s spherical joints, Matrix $\mathbf{N}_\mathrm{L}$ remains same as that given in (51) for a system with only one-DOF joints, while $\mathbf{N}_\mathrm{D}$ changes to the $6n \times (r+3s)$ block diagonal matrix, where r and s represent the number of one-DOF revolute/prismatic joints and three-DOF spherical joints, respectively. Hence, $\mathbf{N}_\mathrm{D}$ is defined by

$$\mathbf{N}_\mathrm{D} \equiv \begin{bmatrix} \mathbf{P}_1 & & & & \\ & \mathbf{P}_2 & & & \\ & & \ddots & & \\ & & & \mathbf{P}_i & \\ & & & & \ddots \\ & & & & & \mathbf{P}_n \end{bmatrix} \tag{17}$$

where $\mathbf{P}_i$ is the joint-motion propagation matrix for the three-DOF spherical joints obtained from (16), or the joint-motion propagation vector for the one-DOF revolute/prismatic joints, $\mathbf{p}_i$ as presented in (49), depending on the ith link connected to its previous one by a three-DOF joint or a one-DOF joint. Accordingly, $\dot{\boldsymbol{\theta}}$ of (47), is defined as the $(r+3s)$-dimensional vector of independent generalized speeds, which contains $\dot{\theta}$'s for revolute/prismatic joints associated to vector $\mathbf{p}$ in matrix $\mathbf{N}_\mathrm{D}$, and $\dot{\mathbf{e}}$'s for spherical joints corresponding to $\mathbf{P}$ elements in matrix $\mathbf{N}_\mathrm{D}$.

The rest remains same for a system with only one-DOF joints and that with one- and three-DOF joints. So far, in deriving (53) for an open-loop serial type system, it is assumed that all the joint variables are independent. For a closed-loop system, this is, however, not true, i.e., all joint variables are not independent. In order to apply the dynamics modeling methodology presented above, the closed-loop system under study is first made open by cutting the appropriate joints and substitute the constraint forces or moments in terms of Lagrange multiplies to maintain kinematic constraints unchanged. As a result, the advantages of the serial chain systems, namely, the development of recursive dynamics algorithms can be exploited [7] even for the closed-loop system. This is done in the following subsection.

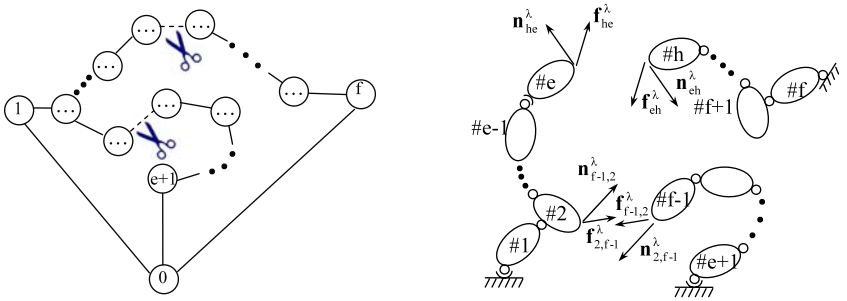

(a) The topology of the closed-loop system (b) The cut joints and Lagrange multipliers

Fig. 4 Reaction forces at the cut joints

3.1 Closed-loop systems

A closed loop is converted here into some open chains, which can be spanning-trees or serial systems, by cutting its appropriate joints. The topology of the linkage, which obtained from graph theory and shown in Fig. 1(b) is employed to find the appropriate joints, which should be cut. It is obvious that the number of cut must be equal to the number of independent closed-loops. Use of concept of cumulative degree of freedom (CDOF) in graph theory identifies the appropriate joints to be cut [16–18] as cited in [19].

The total DOF of all joints lie in an open chain, namely the branch of the tree, is called the CDOF. Using this concept, one should cut the joints such that the maximum CDOF of all branches is minimum. After choosing the joints being cut, links can be numbered properly.

The links of initial closed-loop system should be numbered in such a way that after cutting the joints, the numbers of the links in each branch of opened systems are consecutive. For example, the schematic linkage shown in Fig. 1 is cut at proper joints to obtain some serial subsystems shown in Fig. 4. If the cuts lead to tree-structure, the method of numbering given in [7] is suitable.

The scissors symbols of Fig. 4(a) indicate the proper joints to be cut, whereas $\mathbf{f}^{\lambda}_{ij}$ and $\mathbf{n}^{\lambda}_{ij}$ in Fig. 4(b) denote the components of the force and moment caused due to the Lagrange multipliers representing generalized reaction forces at the cut joints.

Since the Lagrange multipliers representing the constraint forces and moments at the cut joints, are treated as external forces and moments applied to the resulting serial subsystems, vector $\mathbf{w}^{\mathrm{e}}$ of (54) should now include the wrenches due to the Lagrange multipliers as well. Let us replace $\mathbf{w}^{\mathrm{e}}$ of (54) with $\mathbf{w}^{\mathrm{e}} + \mathbf{w}^{\lambda}$ to distinguish the true external wrenches, $\mathbf{w}^{\mathrm{e}}$, from those due to the Lagrange multipliers, $\mathbf{w}^{\lambda}$. For every open loop, which obtained by cutting a closed-loop system, (53), is then modified to [7]

$$\mathbf{N}_j^{\mathrm{T}}(\mathbf{M}_j\dot{\mathbf{t}}_j + \mathbf{W}_j\mathbf{M}_j\mathbf{E}_j\mathbf{t}_j) = \mathbf{N}_j^{\mathrm{T}}\left(\mathbf{w}_j^{\mathrm{e}} + \mathbf{w}_j^{\lambda}\right) \tag{18}$$

where j stands for the opened subsystems, and all the matrices and vectors are with appropriate dimensions. Now, the equations of motion for the whole system taking into account all the opened subsystems can be written as

$$\mathbf{N}^{\mathrm{T}}(\mathbf{M}\dot{\mathbf{t}} + \mathbf{WME}\mathbf{t}) = \mathbf{N}^{\mathrm{T}}\left(\mathbf{w}^{\mathrm{e}} + \mathbf{w}^{\lambda}\right) \tag{19}$$

in which the associated vectors and matrices are

$$\mathbf{M} = \text{diag}[\mathbf{M}_\text{I} \quad \mathbf{M}_\text{II} \quad \dots \quad \mathbf{M}_\text{O}]; \qquad \mathbf{W} = \text{diag}[\mathbf{W}_\text{I} \quad \mathbf{W}_\text{II} \quad \dots \quad \mathbf{W}_\text{O}]$$
$$\mathbf{N}_\text{L} = \text{diag}[\mathbf{N}_\text{LI} \quad \mathbf{N}_\text{LII} \quad \dots \quad \mathbf{N}_\text{LO}]; \qquad \mathbf{N}_\text{D} = \text{diag}[\mathbf{N}_\text{DI} \quad \mathbf{N}_\text{DII} \quad \dots \quad \mathbf{N}_\text{DO}] \tag{20}$$
$$\mathbf{E} = \text{diag}[\mathbf{E}_\text{I} \quad \mathbf{E}_\text{II} \quad \dots \quad \mathbf{E}_\text{O}]$$

and

$$\mathbf{t} = \left[\mathbf{t}_\text{I}^\text{T} \quad \mathbf{t}_\text{II}^\text{T} \quad \dots \quad \mathbf{t}_\text{O}^\text{T}\right]^\text{T}; \qquad \mathbf{w}^\text{e} = \left[\mathbf{w}_\text{I}^{\text{e}^\text{T}} \quad \mathbf{w}_\text{II}^{\text{e}^\text{T}} \quad \dots \quad \mathbf{w}_\text{O}^{\text{e}^\text{T}}\right]^\text{T}$$
$$\mathbf{w}^\lambda = \left[\mathbf{w}_\text{I}^{\lambda^\text{T}} \quad \mathbf{w}_\text{II}^{\lambda^\text{T}} \quad \dots \quad \mathbf{w}_\text{O}^{\lambda^\text{T}}\right]^\text{T} \tag{21}$$

Matrices $\mathbf{M}_\text{I}$, $\mathbf{M}_\text{II}$, and $\mathbf{M}_\text{O}$ are the generalized mass matrices, as defined in (46), for the opened subsystems. Other matrices and vectors are similarly defined.

Next, it is shown how to obtain the reactions at the uncut joints. These may be required for mechanical design and force/moment optimization purposes. The algorithm for the open-loop system proposed in [21], is presented here, namely

$$\mathbf{w}_{i-1,i} = \mathbf{A'}_{i,i+1}\mathbf{w}_{i,i+1} + \mathbf{w}_i^* - \mathbf{w}_i^\text{e} \tag{22}$$

in which

$$\mathbf{w}_{i-1,i} \equiv \begin{bmatrix} \mathbf{n}_{i-1,i} \\ \mathbf{f}_{i-1,i} \end{bmatrix}; \qquad \mathbf{w}_i^* \equiv \begin{bmatrix} \mathbf{n}_i^* \\ \mathbf{f}_i^* \end{bmatrix} \quad \text{and} \quad \mathbf{A'}_{i,i+1} \equiv \begin{bmatrix} \mathbf{1} & \tilde{\mathbf{a}}_{i,i+1} \\ \mathbf{O} & \mathbf{1} \end{bmatrix} \tag{23}$$

where the moment, $\mathbf{n}_{i-1,i}$, and the force, $\mathbf{f}_{i-1,i}$, are those applied by the $(i-1)$st body to the ith one at the ith joint, and $\mathbf{w}_i^*$ introduces the inertia wrench of the ith body as $\mathbf{M}_i\dot{\mathbf{t}}_i + \mathbf{W}_i\mathbf{M}_i\mathbf{E}_i\mathbf{t}_i \equiv \mathbf{w}_i^*$. In (22), the 6×6 matrix, $\mathbf{A'}_{i,i+1}$, is the wrench-propagation matrix which transforms the wrench acting at point O_{i+1} to O_i of the ith body.

4 Case studies

In this section, the algorithm is applied to two examples. These are: (i) a spatial revolute-spherical–spherical-revolute (RSSR) linkage, and (ii) a half model of suspension and steering linkage of a commercial passenger car. With the former system, i.e., the RSSR linkage, it may be possible to show that the proposed algorithm is faster compared to the conventional consideration of a spherical joint as three intersecting revolute joint, as done in [7].

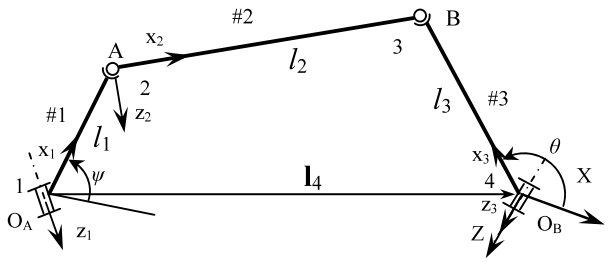

Fig. 5 Four-bar RSSR mechanism

4.1 RSSR mechanism

The four-bar RSSR linkage, as shown in Fig. 5, is considered first whose links are numbered as #1, . . . , #4, and joints by 1, . . . , 4. This system was analyzed in [7, 9], where the spherical joints are treated as three intersecting revolute joints. In this paper, the same methodology is adopted except that the spherical joint motions are represented using the Euler parameters. Correspondingly, changes are made in the derivation of the DeNOC matrices, as shown in subsequent paragraphs.

4.1.1 Kinematic analysis

Since the DeNOC matrices themselves are function of the link orientations, their evaluation methodology is explained as follows:

Using Kutzbach criterion [14] the degree of freedom (DOF) of the RSSR linkage is two, of which, one is the rotation of input link, #1, denoted as ψ, and the other one is the rotation of coupler #2 about its own axis, which is called redundant DOF because it does not affect the input/output rotation. As depicted in Fig. 5, three Cartesian coordinate systems are attached to #1, #2, and #3 as explained in Sect. 2. Note that the fixed reference frame is considered at joint 4, which is attached to the fixed base and whose X-axis is along the common perpendicular of two revolute joints, namely, joints 1 and 4, and global Z-axis is along the axis of joint 4. Since #1 rotates about constant axis of z_1, let us define $\mathbf{B}_1$ to denote the transformation of $x_1y_1z_1$ w.r.t. XYZ. In this rotation matrix, only ψ, the angle of #1 as shown in Fig. 5, is variable.

Next, the rotation of frame $x_2y_2z_2$ w.r.t. $x_1y_1z_1$ is defined using the Euler parameters, as #2 is connected to #1 by a spherical joint. It is represented by $\mathbf{B}_{21}$, i.e.,

$$\mathbf{B}_{21} = \big(2e_{02}^2 - 1\big)\mathbf{1} + 2\big(\mathbf{e}_2\mathbf{e}_2^{\mathrm{T}} + e_{02}\tilde{\mathbf{e}}_2\big) \tag{24}$$

where $[e_{02} \quad \mathbf{e}_2^{\mathrm{T}}]^{\mathrm{T}} \equiv \mathbf{p}_{\mathbf{e}21}$ are the Euler parameters of the second moving frame, $x_2y_2z_2$, w.r.t. the first moving frame, $x_1y_1z_1$.

In view of the fact that #3 rotates in the XY plane about Z axis, the rotation of $x_3y_3z_3$ w.r.t. XYZ is easily written and termed $\mathbf{B}_4$.

Note that for the given values of the input angle, ψ, there are five unknowns, namely, e_{02}, three components of $\mathbf{e}_2$, and θ that need to be obtained to define the configurations of all the four-bar linkage completely. The five unknowns are solved from the five constraint equations that are expressed in the form of (7), where the scalar five equations are obtained as follows:

- Three components of the kinematic loop closure equations being

$$\begin{bmatrix} \phi_1 \\ \phi_2 \\ \phi_3 \end{bmatrix} = \mathbf{B}_1 \begin{bmatrix} l_1 \\ 0 \\ 0 \end{bmatrix} + \mathbf{B}_1\mathbf{B}_{21} \begin{bmatrix} l_2 \\ 0 \\ 0 \end{bmatrix} - \begin{bmatrix} l_{4x} \\ l_{4y} \\ l_{4z} \end{bmatrix} - \mathbf{B}_4 \begin{bmatrix} l_3 \\ 0 \\ 0 \end{bmatrix} \tag{25}$$

  where $[l_1\ 0\ 0]^{\mathrm{T}}$ indicates point A in the first moving coordinate system, while $[l_2\ 0\ 0]^{\mathrm{T}}$ and $[l_3\ 0\ 0]^{\mathrm{T}}$ represent point B in the second and third moving coordinate systems, respectively, and the 3-dimensional vector $\mathbf{l}_4 \equiv [l_{4x}\ l_{4y}\ l_{4z}]^{\mathrm{T}}$ represents the position of $\mathrm{O_B}$ w.r.t. $\mathrm{O_A}$ in global frame, as shown in Fig. 5.

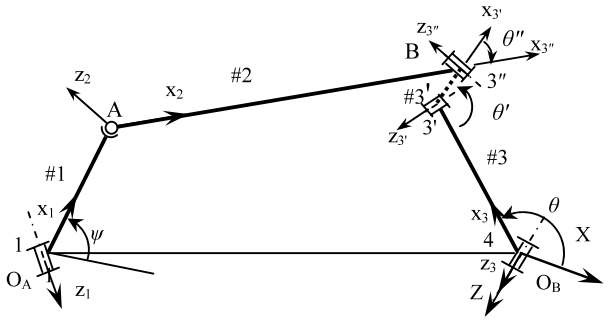

Fig. 6 Four-bar RSRRR mechanism

- The constraint ϕ_4 being dependency of the Euler parameters, (2), i.e.,

$$\phi_4 = \mathbf{p}_{\mathbf{e}21}^{\mathrm{T}} \mathbf{p}_{\mathbf{e}21} - 1 \tag{26}$$

- The last constraint is due to the elimination of the redundant DOF in #2. As shown in Fig. 6, the spherical joint at point B is replaced by two revolute joints. The length of the imaginary link #3′ connecting the joints 3′ and 3″ is taken as zero, whereas the axis of joint 3′, z_3', is considered parallel to the Z-axis of fixed frame, and the axis of joint 3″, z_3'', is taken orthogonal to both z_3' and x_2. Now, the z axis of the second moving frame is defined parallel to z_3''. Since, $x_2 y_2 z_2$ is parallel to $x_3'' y_3'' z_3''$, $\mathbf{B}_2$ should be equal to $\mathbf{B}_3''$. In other words, $\mathbf{B}_1 \mathbf{B}_{21} = \mathbf{B}_3 \mathbf{B}^{3'3} \mathbf{B}_{3''3'}$ or $\mathbf{B}_l = \mathbf{B}_r$, where l and r stand for left and right sides of the expression, respectively. Since in this case, $\mathbf{B}_r(3,3)$ is equal to zero, this element is taken as the last constraint equation. The equation is

$$\phi_5 = \mathbf{B}_l(3,3) \tag{27}$$

Referring to (7) for the linkage at hand, $\mathbf{q} \equiv [\mathbf{o}^{\mathrm{T}} \quad \psi]^{\mathrm{T}}$ is the 6-dimensional vector of generalized coordinates for the RSSR mechanism at hand, whereas $\mathbf{o} \equiv [e_{02} \ \mathbf{e}_2^{\mathrm{T}} \ \theta]^{\mathrm{T}}$ is the 5-dimensional vector array of dependent coordinates. The term ψ is the independent coordinate for the one-DOF RSHR mechanism. To derive the generalized velocities and acceleration for the RSSR mechanism whose dimensions are given in Table 1, the constraint equations, namely (25)–(27), are differentiated with respect to (w.r.t.) time as they were presented in Sect. 2. The input, ψ, is taken as a linear function of time that varies between 0 and 2π, in $t = 0.6$ sec., where position analysis results are given in Fig. 7. In order to validate the results, a separate CAD model is developed in ADAMS (Advanced Dynamic Analysis of Mechanical System) software environment. The outputs of the ADAMS model are also shown in Fig. 7, which indicate good agreement of the analytical results and results taken from ADAMS.

4.1.2 Dynamics analysis

In order to obtain dynamics results using the DeNOC matrices, the RSSR linkage, shown in Fig. 6, is first made open by cutting joint 3, located at point B. It is then substituted with appropriate Lagrange multiplies. Due to this cut, the closed-loop system is now converted to two open-loop systems. As it was pointed out in Sect. 4.1.1, joint 3 is treated as two intersecting revolute joints. Hence after cutting, there will be three reaction forces, as the scalar components of $\mathbf{f}_{23}^{\lambda}$, and a reaction moment about the axis of #2, which is the only

Table 1 Dimensions, mass, and inertia properties of the RSSR linkage and the CPU time

Link	Length (mm)	Variable	Initial values	Joint axis	Joint coord. (mm)	Mass (gr)	Inertia matrix in local frame (kg-m^2)	Rotation matrix of initial position
1	50	Ψ	0°	$\begin{bmatrix} 0 \\ -0.5 \\ 0.866 \end{bmatrix}$	$\begin{bmatrix} -130 \\ -20 \\ -20.36 \end{bmatrix}$	45	$\begin{bmatrix} 7.5 & 0 & 0 \\ 0 & 379 & 0 \\ 0 & 0 & 379 \end{bmatrix} \times 10^{-7}$	$\mathbf{B}_{10} = \begin{bmatrix} 1 & 0 & 0 \\ 0 & 0.866 & -0.5 \\ 0 & 0.5 & 0.866 \end{bmatrix}$
2	110		0.766	—	—	91		—
		e_{02}	$\begin{bmatrix} -0.188 \\ -0.258 \\ 0.558 \end{bmatrix}$				$\begin{bmatrix} 1.53 & 0 & 0 \\ 0 & 371 & 0 \\ 0 & 0 & 371 \end{bmatrix} \times 10^{-6}$	
		$\mathbf{e}_2$						
3	100	θ	122°	$\begin{bmatrix} 0 \\ 0 \\ 1 \end{bmatrix}$	$\begin{bmatrix} 0 \\ 0 \\ 0 \end{bmatrix}$	84	$\begin{bmatrix} 1.4 & 0 & 0 \\ 0 & 281 & 0 \\ 0 & 0 & 281 \end{bmatrix} \times 10^{-6}$	—

CPU time of dynamic analysis of RSSR linkage using the proposed algorithm for 1000 steps 0.438 sec

CPU time of dynamic analysis of RSSR linkage using the revolute joints substitution and the DeNOC matrices for 1000 steps 0.486 sec

The percentage of being faster for the proposed method $\approx$ 10%

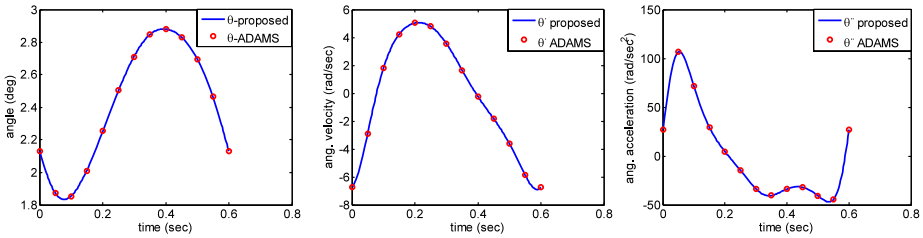

(a) Output angle, θ of #3, and its time derivatives

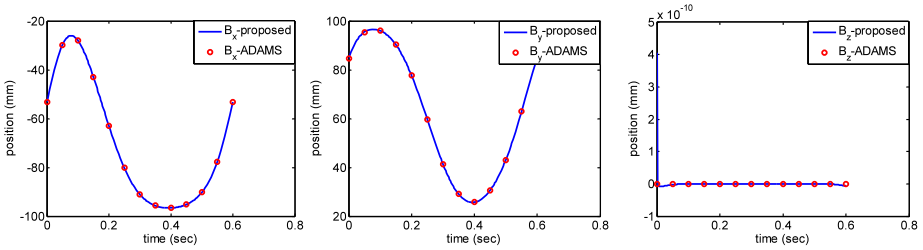

(b)The x, y, and z components of point B

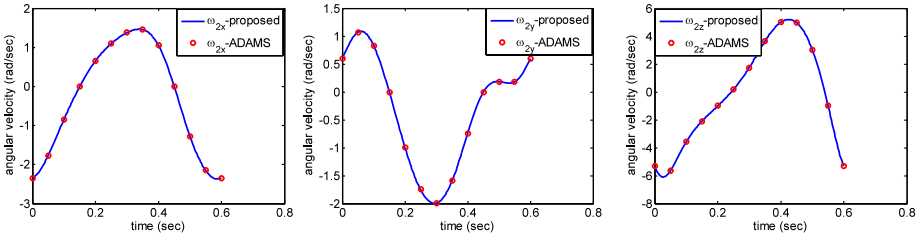

(c) The x, y, and z components of angular velocity of #2

Fig. 7 Numerical and ADAMS kinematic results of the RSSR linkage analysis

component of $\mathbf{n}_{23}^{\lambda}$. The DeNOC matrices for the two open subsystems are then combined to yield the following:

$$\mathbf{N}_{\mathrm{L}} = \begin{bmatrix} \mathbf{1} & \mathbf{O} & \mathbf{O} \\ \mathbf{A_{21}} & \mathbf{1} & \mathbf{O} \\ \mathbf{O} & \mathbf{O} & \mathbf{1} \end{bmatrix}; \qquad \mathbf{N}_{\mathrm{D}} = \begin{bmatrix} \mathbf{p_1} & \mathbf{O} & \mathbf{0} \\ \mathbf{0} & \mathbf{P_2} & \mathbf{0} \\ \mathbf{0} & \mathbf{O} & \mathbf{p_3} \end{bmatrix} \tag{28}$$

where $\mathbf{N}_{\mathrm{L}}$ and $\mathbf{N}_{\mathrm{D}}$ are 18×18 and 18×5 matrices corresponding to the 18-dimensional generalized twist, $\mathbf{t}$ of (47), and the 5-dimensional joint rate vector $\dot{\boldsymbol{\theta}}$ given by $\dot{\boldsymbol{\theta}} \equiv [\dot{\psi}\ \dot{\mathbf{e}}_2^{\mathrm{T}}\ \dot{\theta}]^{\mathrm{T}}$.

Now, referring to Fig. 8 and neglecting the gravity forces, the wrench associated with external forces for the left side, i.e., $\mathrm{O_A AB}$, is given by

$$\mathbf{w}_l^{\mathrm{e}} = \left[\mathbf{w}_1^{\mathrm{e}^{\mathrm{T}}} \quad \mathbf{w}_2^{\mathrm{e}^{\mathrm{T}}}\right]^{\mathrm{T}} \tag{29}$$

in which $\mathbf{w}_1^{\mathrm{e}}$ and $\mathbf{w}_2^{\mathrm{e}}$ are the 6-dimensional vector of external wrenches at joints 1 and 2, respectively. The vectors $\mathbf{w}_1^{\mathrm{e}}$ and $\mathbf{w}_2^{\mathrm{e}}$ are defined as

$$\mathbf{w}_1^{\mathrm{e}} \equiv \left[(\mathbf{u}_1 \tau)^{\mathrm{T}} \quad \mathbf{0}\right]^{\mathrm{T}} \quad \text{and} \quad \mathbf{w}_2^{\mathrm{e}} = \mathbf{0} \tag{30}$$

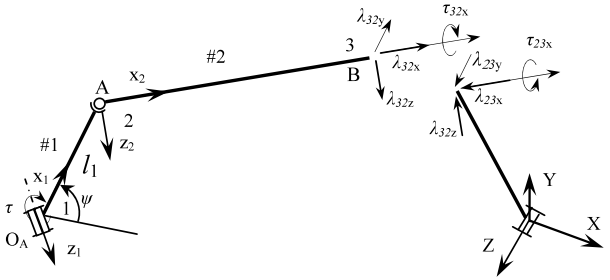

Fig. 8 Reaction forces at cut joint B

where τ is the actuating torque applied to #1 at revolute joint 1 and $\mathbf{u}_1$ is the unit vector along z_1 of joint 1. The next term on the right-hand side of (19) is the wrench associated with the Lagrange multipliers due to cutting of joint B, which is found for the left open chain as

$$\mathbf{w}_l^{\lambda} = \begin{bmatrix} \mathbf{w}_1^{\lambda^{\mathrm{T}}} & \mathbf{w}_2^{\lambda^{\mathrm{T}}} \end{bmatrix}^{\mathrm{T}} \tag{31}$$

in which $\mathbf{w}_1^{\lambda}$ and $\mathbf{w}_2^{\lambda}$ are the 6-dimensional wrenches associated with the Lagrange multipliers at the joints 1 and 2, respectively. Note that the Lagrange multipliers due to cut joint 3, i.e., λ_{32x}, λ_{32y}, λ_{32z}, and τ_{32x} must be expressed with respect to the origin of link 2, namely, point A, and in the fixed frame. Hence, they are given as $\mathbf{w}_1^{\lambda} = \mathbf{0}$ and $\mathbf{w}_2^{\lambda} = \mathbf{A}'_{23}\mathbf{w}_3^{\lambda}$, where $\mathbf{w}_3^{\lambda} = \mathbf{B}\mathbf{w}_3'^{\lambda}$ in which $\mathbf{w}_3'^{\lambda}$ is defined in the second moving frame and is $\mathbf{w}_3'^{\lambda} \equiv [\tau_{32x}\ 0\ 0\ \lambda_{32x}\ \lambda_{32y}\ \lambda_{32z}]^{\mathrm{T}}$, and $\mathbf{B}$ is the rotation matrix that converts the wrench associated with the Lagrange multipliers of the left chain from the moving frame to fixed frame. Thus, one can write (31) as

$$\mathbf{w}_l^{\lambda} = \mathbf{A}'\mathbf{B}\mathbf{w}_3'^{\lambda} \tag{32}$$

where the 12×6 matrix $\mathbf{A}'$, the 6×6 matrix $\mathbf{A}'_{23}$, and the 6×6 matrix $\mathbf{B}$ are given by

$$\mathbf{A}' \equiv \begin{bmatrix} \mathbf{O} \\ \mathbf{A}'_{23} \end{bmatrix}, \qquad \mathbf{A}'_{23} \equiv \begin{bmatrix} \mathbf{1} & \tilde{\mathbf{a}}_{23} \\ \mathbf{O} & \mathbf{1} \end{bmatrix} \quad \text{and} \quad \mathbf{B} = \begin{bmatrix} \mathbf{B}_1\mathbf{B}_{21} & \mathbf{O} \\ \mathbf{O} & \mathbf{B}_1\mathbf{B}_{21} \end{bmatrix} \tag{33}$$

Now, it a simple matter to find the wrench associated with external forces for the right side chain, i.e., O_BB, as

$$\mathbf{w}_r^{\mathrm{e}} = \mathbf{w}_3^{\mathrm{e}} \quad \text{where } \mathbf{w}_3^{\mathrm{e}} = \mathbf{0} \tag{34}$$

Moreover, the wrench associated with the Lagrange multipliers for this chain is

$$\mathbf{w}_r^{\lambda} = \mathbf{A}'_{43}\mathbf{B}_3\left(-\mathbf{w}_3'^{\lambda}\right) \tag{35}$$

in which $\mathbf{A}'_{43}$ is defined similar to $\mathbf{A}'_{23}$. After all, the 18×1 vectors of $\mathbf{w}^{\mathrm{e}}$ and $\mathbf{w}^{\lambda}$ for the whole linkage are obtained from (20) as

$$\mathbf{w}^{\mathrm{e}} = \begin{bmatrix} \mathbf{w}_l^{\mathrm{e}^{\mathrm{T}}} & \mathbf{w}_r^{\mathrm{e}^{\mathrm{T}}} \end{bmatrix}^{\mathrm{T}} \quad \text{and} \quad \mathbf{w}^{\lambda} = \begin{bmatrix} \mathbf{w}_l^{\lambda^{\mathrm{T}}} & \mathbf{w}_r^{\lambda^{\mathrm{T}}} \end{bmatrix}^{\mathrm{T}} \tag{36}$$

Finally, all the matrices associated with dynamic equations of motion of the RSSR mechanism, namely (19), are known. It is pointed here that all equations are expressed in the fixed frame, i.e., XYZ. Hence, the inertia matrices for #1, #2, and #3 are accordingly calculated

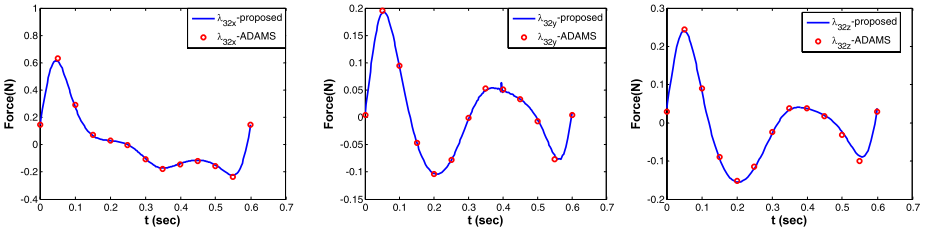

(a) The x, y, and z components of reaction force at joint 3

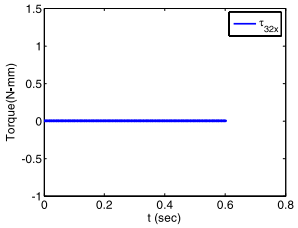

(b) Reaction torque at joint 3

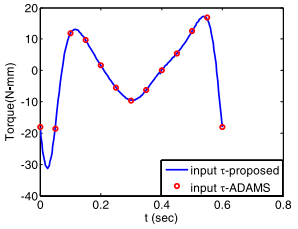

(c) Driving torque at joint 1

Fig. 9 Dynamics results of the RSSR linkage

in the fixed frame. Furthermore, the joint-motion propagation matrix of spherical joint 2, matrix $\mathbf{P}_2$, in global frame is as follows:

$$\mathbf{P}_2 \equiv \begin{bmatrix} \mathbf{B}_1\mathbf{B}_{21}\mathbf{G}_2^* \\ \mathbf{O} \end{bmatrix} \tag{37}$$

From (19) and (28)–(36), it is now obvious that there are five unknown, which are τ, the actuating torque on #1 at joint 1, τ_{32x}, the reaction torque at joint 3, and the three reaction forces at joint 3 denoted as λ_{32x}, λ_{32y}, and λ_{32z}, in addition five dynamic equations of motion. Hence, a unique set of solution exists, for which the results are shown in Fig. 9.

As it is expected, τ_{32x} is always zero in Fig. 9(b) because there is no force or moment on #2 to be applied or arising because of the kinematic constraints. The dynamics results of the RSSR linkage obtained from the proposed algorithm are also compared with those from the ADAMS model. They show extremely close match. To verify the efficiency of the proposed algorithm, based on Euler parameters of a spherical joint, with that of three intersecting revolute joints substituted for a spherical joint [7], CPU times to run the corresponding computer codes in PIV-3.4 GHZ computer are obtained and reported in Table 1. The shorter CPU times given in Table 1 proves the efficiency of the proposed methodology, where the motion of a spherical joint is specified using the Euler parameters.

4.2 Suspension and steering linkage

In this subsection, the suspension and steering linkage of a commercial passenger car is modeled as a more complicated linkage to show the generality of the proposed algorithm. A CAD model of this linkage is shown in Fig. 10.

This linkage consists of a rack, two tie rods, two steering arms connected to wheel hubs, two struts and two lower arms, and two springs and shock absorbers applying forces to lower and higher parts of the struts. Figure 11(a) shows the scheme of left half of the linkage whose topology obtained from graph theory is shown in Fig. 11(b).

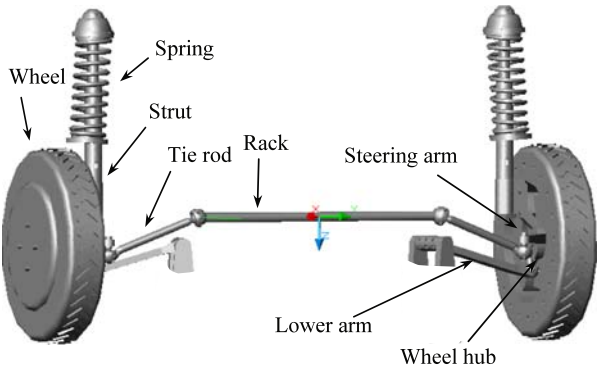

Fig. 10 CAD model of suspension and steering linkage

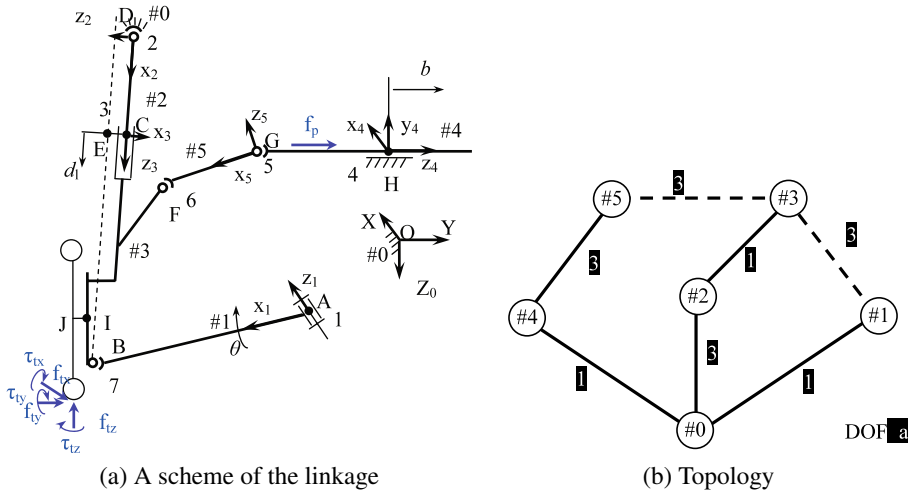

(a) A scheme of the linkage (b) Topology

Fig. 11 The suspension and steering linkage

The topology shows two independent close-loops. Hence, two joints must be cut to open the linkage completely. The highlighted numbers on the lines indicating the joints, represent their DOF. As it is pointed out in Sect. 3, the CDOF of every branch should be minimum after cutting.

Hence, the proper joints for cutting are the spherical joints between #1 and #3, and #3 and #5, where the maximum CDOF is four. It is a simple matter to check that by cutting other two joints, the maximum CDOF is same as four or more. The links of the linkage are numbered in such a way that after cutting and converting the closed loop to three serial chains, the link numbers of every serial chain are consecutive.

Some representative results of the suspension and steering linkage analysis are shown in Fig. 12. The figure shows the force applied to the rack to move it by a sine function for maximum rack travel in two sec. The force applied to the tire is same as the sample given in [22]. The details of the modeling and results are avoided here to keep the size of paper reasonable. The modeling details of the suspension and steering linkage will be communicated later as a separate submission.

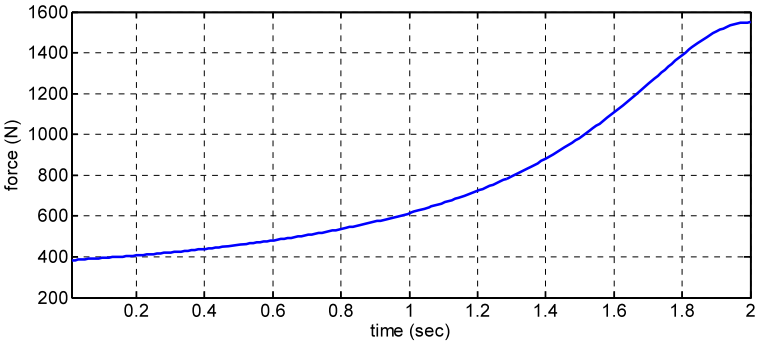

Fig. 12 The force applied to the rack of the suspension and steering linkage

5 Conclusions

In this work, the dynamic modeling of multibody systems with spherical joints whose motions are described using Euler parameters is presented. In general, a spherical joint is modeled as three intersecting orthogonal revolute joints with zero intermediate link lengths. The later procedure causes the increase in the sizes of the associated matrices. To avoid the unnecessary introduction of the intermediate links and increasing the matrix dimensions, the Euler parameters are employed to represent the motion of a link connected to the previous one by a spherical joint. Correspondingly, the Decoupled Natural Orthogonal Complement (DeNOC) matrices used for the development of dynamic algorithms are modified. To confirm the efficiency of the proposed representation, a spatial four-bar Revolute-Spherical–Spherical-Revolute (RSSR) mechanism is analyzed and compared to that one reported in the literature [7]. The CPU times in Table 1 show almost 10% improvement. Besides, less computer memory is required using the proposed methodology due to the smaller matrix sizes.

Finally, the contributions of this paper are highlighted as:

(1) Extension of the concept of the DeNOC matrices for the multibody systems with spherical joints using Euler parameters to denote their motions.
(2) Verification of the efficiency of the dynamic algorithm, particularly, for the RSSR linkage.
(3) Brief explanation of the dynamic analysis of a complex suspension and steering linkage.

Acknowledgements The authors acknowledge Dr. Himanshu Chaudhary who allowed using his code on RSSR linkage analysis being based on three orthogonally intersecting revolute joint substitution for the comparison of the two algorithms.

Appendix

This appendix explains DeNOC matrices for a serial multibody system with only one-DOF joint. Using Euler and Newton laws, equations of motion for the ith body of an open chain can be written as (see Fig. 13)

$$\mathbf{n}_i^C = \mathbf{I}_i^C \dot{\boldsymbol{\omega}}_i + \dot{\mathbf{I}}_i^C \boldsymbol{\omega}_i = \mathbf{I}_i^C \dot{\boldsymbol{\omega}}_i + \tilde{\boldsymbol{\omega}}_i \mathbf{I}_i^C \boldsymbol{\omega}_i \tag{38}$$

$$\mathbf{f}_i^C = m_i \dot{\mathbf{v}}_i^C \tag{39}$$

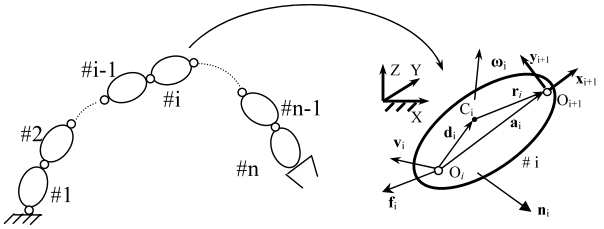

Fig. 13 An n-link serial manipulator

where $\boldsymbol{\omega}_i$, $\mathbf{v}_i^C$, $\mathbf{n}_i^C$ and $\mathbf{f}_i^C$ are 3-dimensional angular velocity, linear velocity, moment, and force vectors, respectively, associated with the ith body and represented about C_i, and $\mathbf{I}_i^C$ and m_i are 3-dimensional inertia matrix about C_i and mass of the body, respectively. If Newton–Euler (NE) equations for the ith body are written about origin O_i, the terms $\dot{\mathbf{v}}_i^C$, $\mathbf{n}_i^C$, $\mathbf{f}_i^C$, and $\mathbf{I}_i^C$ need to be substituted with $\dot{\mathbf{v}}_i$, $\mathbf{n}_i$, $\mathbf{f}_i$, and $\mathbf{I}_i$, which are given as

$$\begin{aligned} &\mathbf{v}_i = \mathbf{v}_i^C + \tilde{\mathbf{d}}_i\boldsymbol{\omega}_i; \qquad \dot{\mathbf{v}}_i = \dot{\mathbf{v}}_i^C + \tilde{\mathbf{d}}_i\dot{\boldsymbol{\omega}}_i + \tilde{\boldsymbol{\omega}}_i\tilde{\mathbf{d}}_i\boldsymbol{\omega}_i \\ &\mathbf{n}_i = \mathbf{n}_i^C + \tilde{\mathbf{d}}_i\mathbf{f}_i^C; \qquad \mathbf{f}_i = \mathbf{f}_i^C \quad \text{and} \quad \mathbf{I}_i = \mathbf{I}_i^C - m_i\tilde{\mathbf{d}}_i^2 \end{aligned} \tag{40}$$

where $\tilde{\mathbf{x}}$ is the 3×3 cross-product matrix associated with the 3-dimensional vector $\mathbf{x}$ so that $\tilde{\mathbf{x}a} = \mathbf{x} \times \mathbf{a}$ for any vector $\mathbf{a}$, and it is defined similar to (4).

On substitution of (40) in (38) and (39), one obtains the following:

$$(\mathbf{I}_i + m_i\tilde{\mathbf{d}}_i^2)\dot{\boldsymbol{\omega}}_i + \tilde{\boldsymbol{\omega}}_i\left(\mathbf{I}_i + m_i\tilde{\mathbf{d}}_i^2\right)\boldsymbol{\omega}_i = \mathbf{n}_i - \tilde{\mathbf{d}}_i\mathbf{f}_i \tag{41}$$

$$m_i\dot{\mathbf{v}}_i - m_i\tilde{\mathbf{d}}_i\dot{\boldsymbol{\omega}}_i - m_i\tilde{\boldsymbol{\omega}}_i\tilde{\mathbf{d}}_i\boldsymbol{\omega}_i = \mathbf{f}_i \tag{42}$$

Equations (41) and (42) are simplified and formed as

$$\mathbf{M}_i\dot{\mathbf{t}}_i + \mathbf{W}_i\mathbf{M}_i\mathbf{E}_i\mathbf{t}_i = \mathbf{w}_i \tag{43}$$

in which the 6×6 matrices, $\mathbf{M}_i$, $\mathbf{W}_i$ and $\mathbf{E}_i$, and the 6-dimensional vectors $\mathbf{t}_i$ and $\mathbf{w}_i$ are given by

$$\begin{aligned} &\mathbf{M}_i \equiv \begin{bmatrix} \mathbf{I}_i & m_i\tilde{\mathbf{d}}_i \\ -m_i\tilde{\mathbf{d}}_i & m_i\mathbf{1} \end{bmatrix}; \qquad \mathbf{W}_i \equiv \begin{bmatrix} \tilde{\boldsymbol{\omega}}_i & \mathbf{O} \\ \mathbf{O} & \tilde{\boldsymbol{\omega}}_i \end{bmatrix}; \qquad \mathbf{E}_i \equiv \begin{bmatrix} \mathbf{1} & \mathbf{O} \\ \mathbf{O} & \mathbf{O} \end{bmatrix}; \\ &\mathbf{t}_i \equiv \begin{bmatrix} \boldsymbol{\omega}_i \\ \mathbf{v}_i \end{bmatrix} \quad \text{and} \quad \mathbf{w}_i \equiv \begin{bmatrix} \mathbf{n}_i \\ \mathbf{f}_i \end{bmatrix} \end{aligned} \tag{44}$$

where $\mathbf{I}_i$ is the 3×3 inertia tensor for the ith body about O_i. The two last vectors, $\mathbf{t}_i$ and $\mathbf{w}_i$, are called twist and wrench of the ith body, respectively.

For a multibody system with n rigid links, the uncoupled NE equations of motion, (43), are then written in a compact form as

$$\mathbf{M}\dot{\mathbf{t}} + \mathbf{WME}\mathbf{t} = \mathbf{w} \tag{45}$$

where the $6n \times 6n$ matrices, $\mathbf{M}$, $\mathbf{W}$, $\mathbf{E}$, and the $6n$-dimensional vectors $\mathbf{t}$ and $\mathbf{w}$ are defined as follows:

$$M \equiv \text{diag}[\mathbf{M}_1, \mathbf{M}_2, \ldots, \mathbf{M}_n]; \qquad \mathbf{W} \equiv \text{diag}[\mathbf{W}_1, \mathbf{W}_2, \ldots, \mathbf{W}_n]$$

$$\mathbf{E} \equiv \text{diag}[\mathbf{E}_1, \mathbf{E}_2, \ldots, \mathbf{E}_n]; \qquad \mathbf{t} \equiv \begin{bmatrix} \mathbf{t}_1^{\mathrm{T}} & \mathbf{t}_2^{\mathrm{T}} & \ldots & \mathbf{t}_n^{\mathrm{T}} \end{bmatrix}^{\mathrm{T}} \quad \text{and} \qquad (46)$$
$$\mathbf{w} \equiv \begin{bmatrix} \mathbf{w}_1^{\mathrm{T}} & \mathbf{w}_2^{\mathrm{T}} & \ldots & \mathbf{w}_n^{\mathrm{T}} \end{bmatrix}^{\mathrm{T}}$$

The twist of the open chain can be written as [3, 6]

$$\mathbf{t} = \mathbf{N}\dot{\boldsymbol{\theta}} \qquad (47)$$

In (47), $\mathbf{N}$ is an orthogonal complement for the coefficient matrix of velocity constraint equations, $\mathbf{A}$, so that $\mathbf{At} = \mathbf{0}$. $\mathbf{N}$ is then termed as Natural Orthogonal Complement (NOC) of $\mathbf{A}$ [6]. In (47), $\dot{\boldsymbol{\theta}} \equiv [\dot{\theta}_1 \quad \ldots \quad \dot{\theta}_n]^{\mathrm{T}}$ is the n-dimensional vector of independent generalized speeds.

Note that the twist of the ith body, $\mathbf{t}_i$, can be expressed in terms of its previous body, i.e., the $(i-1)$st one [3, 20], as

$$\mathbf{t}_i = \mathbf{A}_{i,i-1}\mathbf{t}_{i-1} + \mathbf{p}_{\mathrm{i}}\dot{\theta}_{\mathrm{i}} \qquad (48)$$

where $\mathbf{A}_{i,i-1}$ is the 6×6 twist-propagation matrix, and $\mathbf{p}_i$ is the 6-dimensional vector of joint-motion propagation, which are given by

$$\mathbf{A}_{i,i-1} \equiv \begin{bmatrix} \mathbf{1} & \mathbf{O} \\ \tilde{\mathbf{a}}_{i,i-1} & \mathbf{1} \end{bmatrix}; \qquad \mathbf{p}_i \equiv \begin{bmatrix} \mathbf{u}_i \\ \mathbf{0} \end{bmatrix} \quad \text{revolute;} \qquad \mathbf{p}_i \equiv \begin{bmatrix} \mathbf{0} \\ \mathbf{u}_i \end{bmatrix} \quad \text{prismatic joints} \qquad (49)$$

In (49), $\tilde{\mathbf{a}}_{i,i-1}$ is the 3×3 cross-product matrix associated with the vector $\mathbf{a}_{i,i-1}$, defining position O_{i-1} from O_i. From Fig. 13, vector $\mathbf{a}_{i,i-1}$ can be obtained as $\mathbf{a}_{i,i-1} \equiv -\mathbf{a}_{i-1} = -\mathbf{d}_{i-1} - \mathbf{r}_{i-1}$. Matrix $\tilde{\mathbf{a}}_{i,i-1}$ is defined similar to (4). Moreover, $\mathbf{O}$ and $\mathbf{1}$ are the 3×3 zero and identity matrices, respectively, whereas, $\mathbf{0}$ is the 3-dimensional vector of zeros. In this paper, **O, 1,** and **0** will be understood as of compatible sizes based on where they appear. Furthermore, $\mathbf{u}_i$ is the 3-dimensional unit vector parallel to the ith joint axis.

The NOC matrix given in (47), $\mathbf{N}$, is decomposed next as

$$\mathbf{N} \equiv \mathbf{N}_{\mathrm{L}}\mathbf{N}_{\mathrm{D}} \qquad (50)$$

Matrices $\mathbf{N}_{\mathrm{L}}$ and $\mathbf{N}_{\mathrm{D}}$ are the $6n \times 6n$ lower block triangular matrix, and the $6n \times n$ block diagonal matrix, respectively. They are found for a chain with only one-DOF revolute/prismatic joints as

$$\mathbf{N}_{\mathrm{L}} = \begin{bmatrix} \mathbf{1} & \mathbf{O} & \cdots & \mathbf{O} \\ \mathbf{A_{21}} & \mathbf{1} & \cdots & \mathbf{O} \\ \vdots & \vdots & \ddots & \vdots \\ \mathbf{A_{n1}} & \mathbf{A_{n2}} & \cdots & \mathbf{1} \end{bmatrix} \quad \text{and} \quad \mathbf{N}_{\mathrm{D}} = \begin{bmatrix} \mathbf{p}_1 & \mathbf{0} & \cdots & \mathbf{0} \\ \mathbf{0} & \mathbf{p}_2 & \cdots & \mathbf{0} \\ \vdots & \vdots & \ddots & \vdots \\ \mathbf{0} & \mathbf{0} & \cdots & \mathbf{p}_{\mathrm{n}} \end{bmatrix} \qquad (51)$$

For serially connected three bodies, namely, i, j, and k, the twist propagation matrices satisfy the following properties:

$$\mathbf{A}_{ij}\mathbf{A}_{jk} = \mathbf{A}_{ik}; \qquad \mathbf{A}_{ii} = \mathbf{1}; \qquad \mathbf{A}_{ij}^{-1} = \mathbf{A}_{ji} \qquad (52)$$

Since in (45), the wrench $\mathbf{w}$, includes all the forces and moments applied on the system, i.e., the external forces and moments, the reaction forces and moments, and those due to gravity,

dissipation, etc., it can be substituted as $\mathbf{w} \equiv \mathbf{w}^{\mathrm{e}} + \mathbf{w}^{\mathrm{c}}$, where $\mathbf{w}^{\mathrm{c}}$ contains the reactions and $\mathbf{w}^{\mathrm{e}}$ contains the rest.

It is well known that the work done by reaction forces is zero, then

$$\mathbf{t}^{\mathrm{T}}\mathbf{w}^{\mathrm{c}} = \dot{\boldsymbol{\theta}}^{\mathrm{T}}\mathbf{N}^{\mathrm{T}}\mathbf{w}^{\mathrm{c}} = \mathbf{0} \tag{53}$$

Since $\dot{\boldsymbol{\theta}}$ is the vector of independent coordinates, $\mathbf{N}^{\mathrm{T}}\mathbf{w}^{\mathrm{c}} = \mathbf{0}$, meaning that if both sides of (45) are premultiplied by $\mathbf{N}^{\mathrm{T}}$, i.e., the transpose of the matrix $\mathbf{N}$, the wrench due to reaction forces and moments are vanished, and (45) yields to

$$\mathbf{N}^{\mathrm{T}}(\mathbf{M}\dot{\mathbf{t}} + \mathbf{WMEt}) = \mathbf{N}^{\mathrm{T}}\mathbf{w}^{\mathrm{e}} \tag{54}$$

Equation (54) is termed as coupled equations of motion for an open-loop serial type system whose all joint variables are assumed to be independent.

References

1. Nikravesh, P.E.: Computer-Aided Analysis of Mechanical Systems. Prentice-Hall, Englewood Cliffs (1988)
2. Garcia de Jalon, J.: Kinematic and Dynamic Simulation of Multibody Systems. Springer, Berlin (1994)
3. Saha, S.K.: A decomposition of manipulator inertia matrix. IEEE Trans. Robotics Autom. **13**(2), 301–304 (1997)
4. Saha, S.K., Schiehlen, W.O.: Recursive kinematics and dynamics for closed loop multibody systems. Mech. Struct. Mach. **2**(29), 143–175 (2001)
5. Huston, R.L., Passerello, C.E.: On constraint equation-A new approach. ASME J. Appl. Mech. **41**, 1130–1131 (1974)
6. Angeles, J., Lee, S.K.: The formulation of dynamical equations of holonomic mechanical systems using a natural orthogonal compliment. ASME J. Appl. Mech. **55**, 243–244 (1988)
7. Chaudhary, H., Saha, S.K.: Constraint wrench formulation for closed-loop systems using two-level recursions. Mech. Des. **129**(12), 1234–1242 (2007)
8. Angeles, J.: On twist and wrench generators and annihilators. In: Proceedings of the NATO-Advanced Study Institution on Computer Aided Analysis of Rigid and Flexible Systems 1, Troia, Portugal, 27 June–9 July 1993
9. Duffy, J.: Displacement analysis of the generalized RSSR mechanism. Mech. Mach. Theory **13**, 533–541 (1978)
10. Rahmani Hanzaki, A., Saha, S.K., Rao, P.V.M.: Dynamics modeling of multibody systems with spherical joints using Euler parameters. In: Proceedings of Multibody Dynamics'2007, ECCOMAS Thematic Conference, Milan, Italy, 25–28 June 2007
11. Robertson, A.P., Slocum, A.H.: Measurement and characterization of precision spherical joints. Precis. Eng. **30**, 1–12 (2006)
12. Attia, H.A.: Dynamic modeling of the double Wishbone motor-vehicle suspension system. Eur. J. Mech. A Solids **21**, 167–174 (2002)
13. Attia, H.A.: Dynamic simulation of constrained mechanical systems using recursive projection algorithm. J. Braz. Soc. Mech. Sci. Eng. **XXVIII**(1), 37–44 (2006)
14. Norton, R.L.: Design of Machinery—An Introduction to the Synthesis and Analysis of Mechanisms and Machines, 2nd edn. McGraw-Hill, New Delhi (2002)
15. Deo, N.: Graph Theory with Application in Engineering and Computer Science. Prentice-Hall, Englewood Cliffs (1974)
16. McPhee, J.J.: On the use of linear graph theory in multibody system dynamics. Nonlinear Dyn. **9**, 73–90 (1996)
17. Smith, D.A.: Reaction force analysis in generalized machine systems. ASME J. Eng. Ind. **95**(2), 617–623 (1973)
18. Milner, J.R., Smith, D.A.: Topological reaction force analysis. ASME J. Mech. Des. **101**(2), 192–198 (1979)
19. Chaudhary, H.: Analysis and optimization of mechanisms with handmade carpets. Ph.D. thesis, Indian Institute of Technology (IIT), Delhi (2007)

20. Saha, S.K.: Dynamic modeling of serial multibody systems using the decoupled natural orthogonal complement matrices. ASME J. Appl. Mech. **66**, 986–996 (1999)
21. Chaudhary, H., Saha, S.K.: Matrix formulation of constraint wrenches for serial manipulators. In: International Conference on Robotics and Automation (ICRA 2005), pp. 4647–4652, Barcelona, Spain, 18–22 April 2005
22. Rahmani Hanzaki, A., Saha, S.K., Rao, P.V.M.: Modeling of a rack and pinion steering linkage using multibody dynamics, In: Proceedings of the 12th IFToMM World Congress, Besançon, France, 18–21 June 2007